PREFLARE OBSERVATIONS

USING THE SKYLAB X-RAY TELESCOPE

by

BONNIE J. BURATTI

Submitted in Partial Fulfilment

of the Requirements for the

Degree of Master of Science

at the

MASSACHUSETTS INSTITUTE OF TECHNOLOGY

February, 1977

Signature of Author _____
Department of Earth and Planetary Sciences, Feb. 4, 1977

Certified by _____
Thesis Supervisor

Accepted by _____
Chairman, Departmental Committee on Graduate Theses

ABSTRACT

In an attempt to better understand the flare build up process, observations of 19 x-ray solar flares prior to their onsets were made. Images from the Skylab x-ray telescope built by American Science and Engineering, Inc. provided unprecedented spatial and temporal resolution of the flare event. Correlation with associated H-α and radio events was done. Almost half the events showed no preflare changes in the active region. In general, energy release was shown to be sudden.

ACKNOWLEDGMENTS

I would like to express my appreciation to Dr. Stephen Kahler of AS&E and Prof. Thomas McCord who advised and encouraged me throughout this work and my graduate school studies. Further encouragement and discussion was provided by Dr. Richard Petrasso, Dr. Allen Krieger, and Dr. Robert Huguenin.

I am also indebted to Dr. David Rust of AS&E for use of Sacramento Peak H-α film, and to Silvio Bichisecchi and Peter Hastings for producing the photographic plates.

TABLE OF CONTENTS

IIST OF FIGURES

CHAPTER I - INTRODUCTION AND SUMMARY

Observation of an active region prior to the onset of a flare are of great importance in understanding the flare build-up process. Previous work for H-α flares yielded a statistical pattern in absorption features 10 - 20 minutes prior to onset. This work attemps to undertake a similar study for x - ray flares, using the Skylab SO - 54 x - ray imaging telescope. Nineteen events are studied and correlations with H-α and radio events are done if possible. Implications for the flare storage and release mechanism are suggested.

A description of the x - ray telescope experiment and its capabilities for studying solar physics is included. Discussion is extended up to the flare rise period to establish any connection between preflare changes and the flare itself.

The results from the study suggest that there is a lack of long term or extensive energy storage in the x - ray region.

CHAPTER II -INSTRUMENTATION

A high resolution x-ray grazing-incidence telescope aboard the Skylab Apollo Telescope Mount produced nearly 35,000 images of the solar disk throughout the period June 1973 to January 1974. The purpose of the experiment was to provide images with high spatial and temporal resolution for investigations into coronal heating mechanism, flare heating mechanisms, flare evolution, bright point formation, distribution and evolution, coronal holes, and the relationship between coronal holes and the solar cycle.

Previous images of the x-ray solar disk were acquired through short rocket flights above the earth's atmosphere and thus gave no data which could be used for long-term or statistical behavior of the sun. During the 10-year program of x-ray rocket flights the resolution of the photographic images has improved from one arc minute to the present 2 arc second on axis accuracy in the Skylab SO - 54 x-ray telescope.[1] Figure 1 shows the progression image quality over the last 10 years. The first image of the sun made with a grazing incidence telescope is shown in a. The image was made October 15, 1963. The last image represents the first successful flight of an x-ray telescope comparable to the Skylab telescope. Technical advances in mirror construction, surface finishing and calibration techniques made in the rocket program, coupled with the less stringent space requirements,has resulted in theimproved resolution. The skylab SO - 54 experiment has a

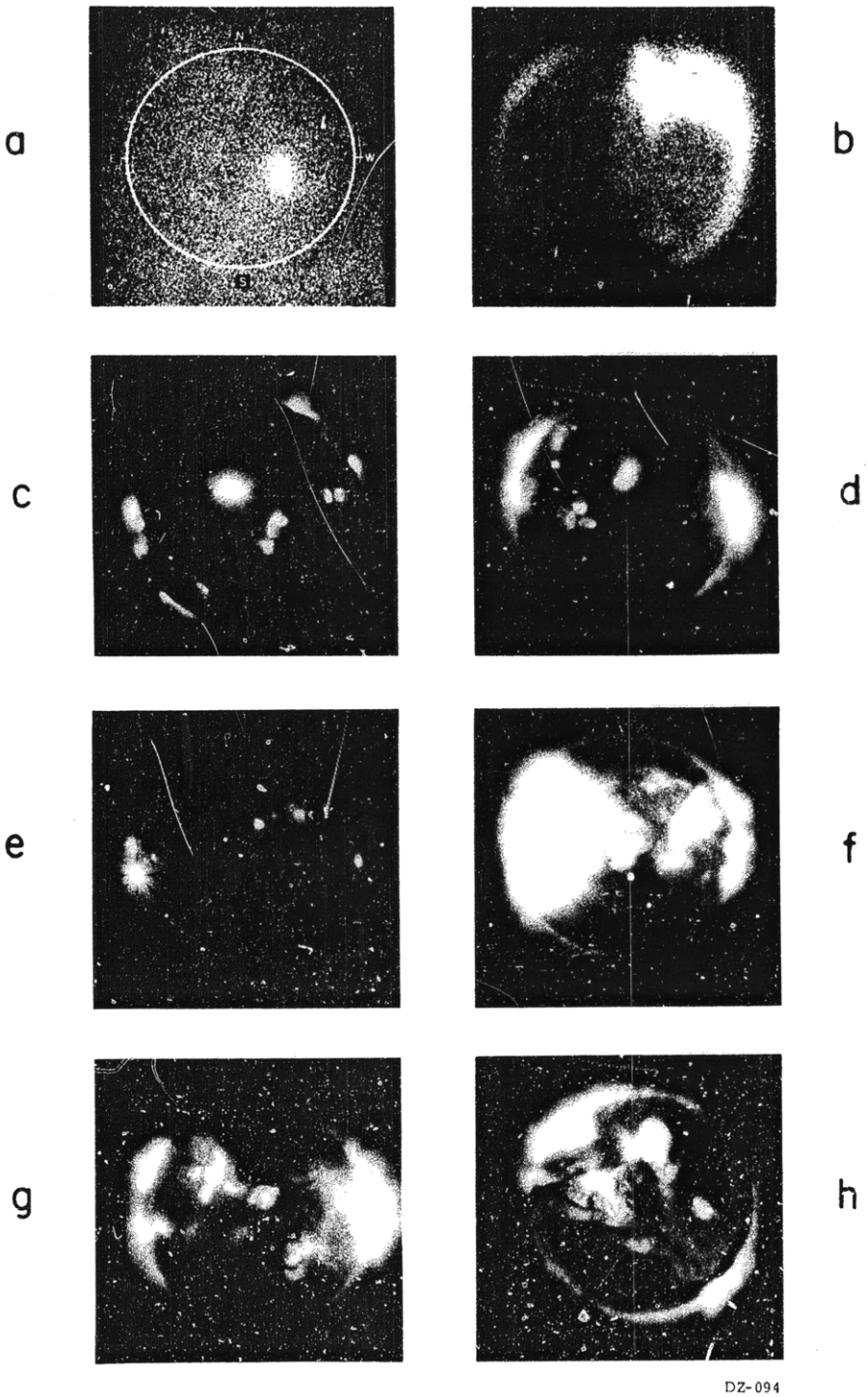

Figure 1

Progress in x-ray solar imaging

larger collecting area because of its larger size and successful use of a nested mirror optics system. The image size itself is larger because of the longer focal length allowed. The film capacity is over one hundred times greater than rocket film capacity.

The wavelength observed by the SO - 54 telescope is in the range 2 - 52 Å. This band pass was chosen because both the resonance line emission from the multiply ionized solar corona and the continuum from the bremstrahlung and hydrogen recombination are in this spectral region. The lower limit is determined by the pitch of the mirror surface to paraxial rays while the longer wavelength limit is imposed by the absorption of the camera magazine window.

Rough spectral information can be acquired by taking ratios of the flux coming through the six filters. A spectrographic grating was also used in the experiment on selected flares and coronal features.

FILTERS

The bandpasses of the six filters range from 2 - 11 Å to 44 - 55 Å. In figure 2 is shown the transmission of the filters as a function of wavelength. The short wavelength bandpasses (filters 1, 5, and 6) are achieved by using beryllium filters of thicknesses 2.67, 4.7 and 9.54 mg cm^{-2}. Two longer wavelength filters are constructed of organic materials transparent to intermediate and longer x-ray wavelengths.

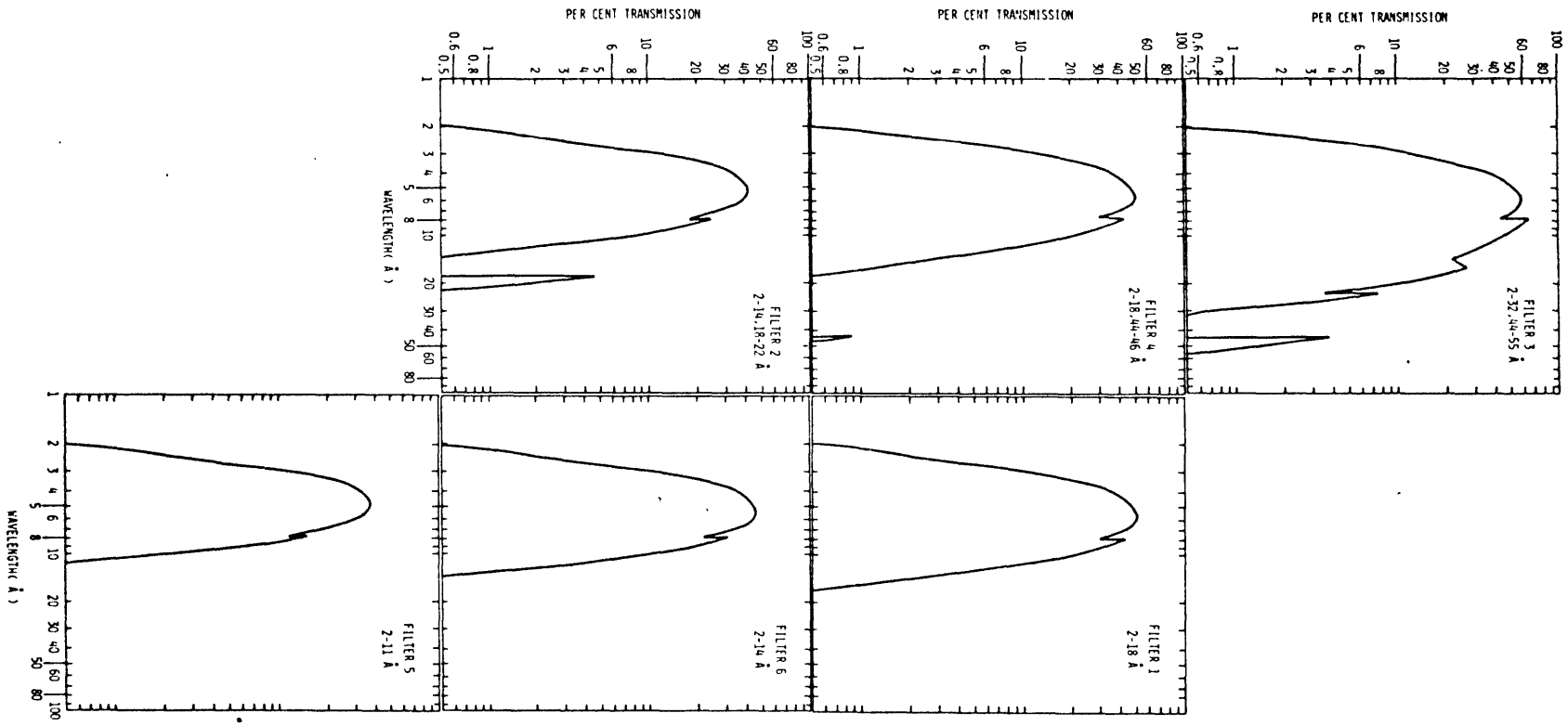

Figure 2 Transmission of the x-ray filters

OPTICS

Giaconni and Rossi made original suggestions of using parboloid mirrors at grazing incidence to obtain images of the x-ray region.[2] Since the radiation is reflected at the far side of the paraboloid, the grazing angle is small and severe chromatic aberration results. A secondary hyperboloid mirror which is coaxial and confocal with the primary reflecting surface compensates the aberration. The existence of only small reflection angles allows for a large ratio of focal length to the diameter of the mirror. "Nesting"the mirror increases the projected frontal surafce. The surfaces of the mirrors are arranged so that the paraboloid's focus and the back focus of the hyperboloid are the same point. This configuration allows focusing after a single reflection on each mirror in the same direction. This design allows a smaller focal length for a given aperature and greater mechanical stability because the surfaces intersect . The surfaces involved in reflection are coated with Kanigen. a nickel-phosphorus alloy, deposited on a beryllium base. Calibrations for the instrument were achieved by pointing the telescope at a few arc second source of soft x-rays at a distance of 220 feet. The experiments have shown that x-ray sources one arc second in diameter separated by two arc seconds are clearly resolved. Figure 3 shows the optical system schematically. The telescope itself is shown in figures 4 and 5.

Before the Skylab x-ray solar experiments (a similar experiment,

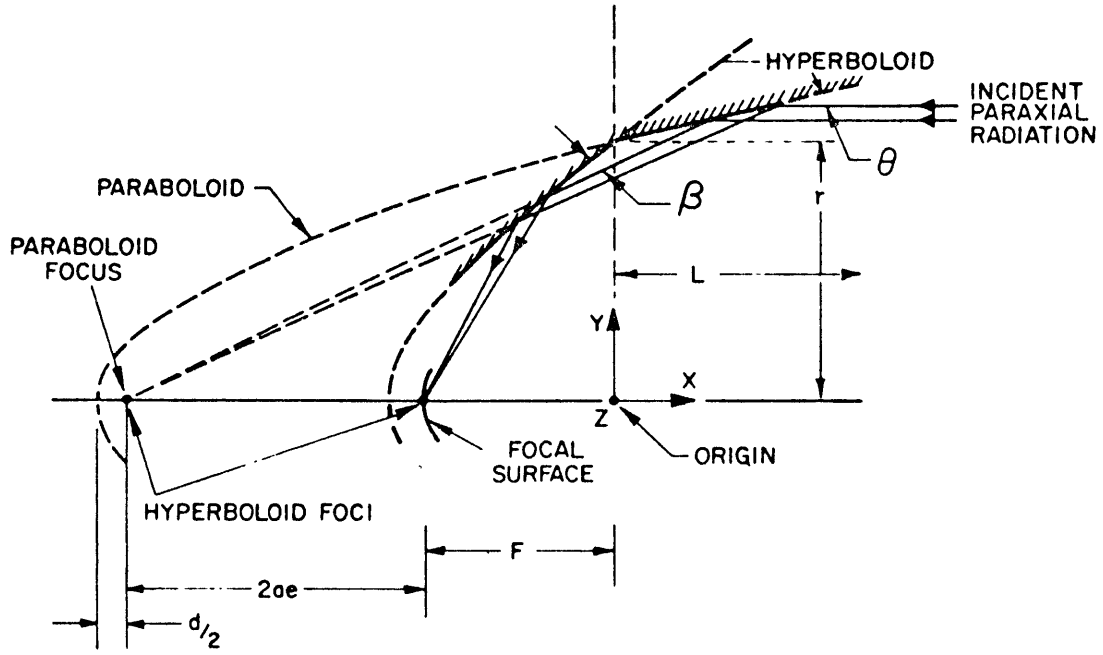

Figure 3

The S-054 telescope optical system

CL-528

Figure 5

The S-054 telescope

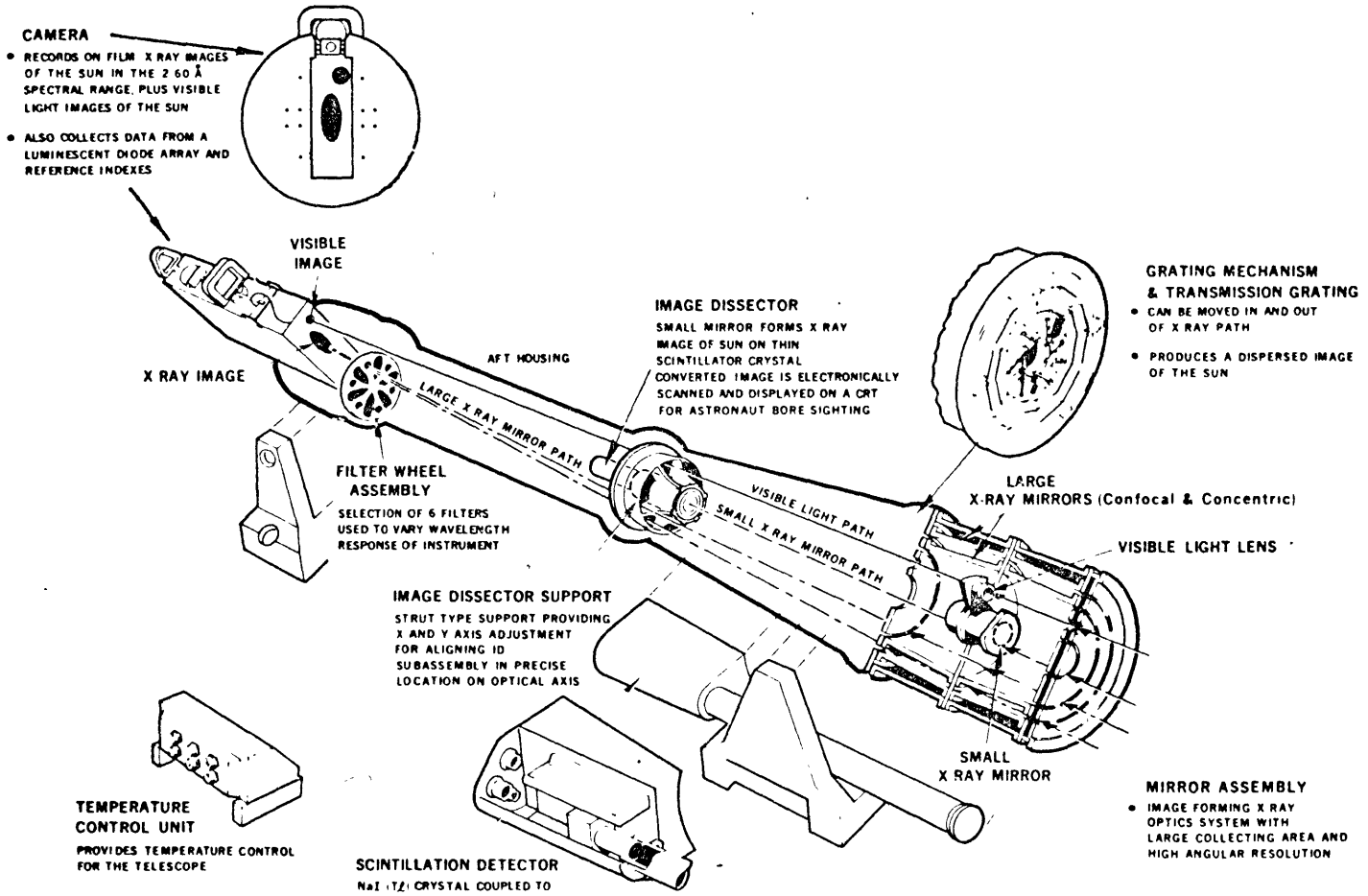

Figure 5 The S-054 telescope - schematic view

the SO - 56 x - ray telescope was developed by Aerospace Corporation and employed on the flight.), no knowledge of the temporal behavior of the sun from five minutes, the duration of the flight, to one year, the time between flights, existed. The Skylab data has provided temporal resolution down to less than a second and consistently over periods of days excluding interuptions for orbiting behind the earth, changing crews, operation of other experiments, or rest periods, for eight months. In addition, during the unmanned portions of the mission the exreriment was on an automatic mode to take highly temporally resolved pictures for about an hour every twelve hours. The existence of such data allows the studies mentioned in the opening paragraph of this chapter, and for this study specifically, the temporal and statistical evolution of flares.

THE X - RAY IMAGES

Results from the rocket experiments indicated that the dynamic range of the solar corona was 10^3. Flare events increase this number by several orders of magnitude. Since the range of the photographic emulsions was only 10^2 - 10^3, a series of exposures each increasing by a factor of four were taken. The exposures in general range from 1/64 - 256 seconds, with 0.35 seconds between each image. In figure 6 is illustrated the sensitivity and range of the experiment. The first graph, which gives the maximum total x-ray emission integral along the line of sight

$$I = \int n_e^2 dl \quad (cm^{-5})$$

as a function of T for each filter, where n_e is the electron density and l is the thickness of the plasma, represents the darkest unsaturated image in the shortest exposure, i.e., the brightest features observable. The other graph gives the minimum integral, which represents the faintest usable image in the longest exposure. In figure 7 is shown the same graph but superimposed with a similar sensitivity plot for two bandpasses on Solrad 9, an orbiting x-ray solar observatory which gives integrated disk profiles for several years, including the time of the Skylab mission. Flare profiles from Solrad proved useful in the present study.

The combination of filters and exposures thus gives a dynamic range of 10^{11}. This range corresponds to a change in electron density from 10^9 - 10^{14} cm^{-3} for an effective scale height of 40,000 km along the line of sight.

A further broadening of the usefulness of the data comes from the ability of the telescope to be operated on one of four modes which can be specified by the existence of varying solar conditions. A flare mode, for example, requires a series of rapidly taken short exposures, whereas a mode of longer exposures can be used to study behavior and evolution of active regions, interconnecting loop structures, or the solar corona. For the present study, the morphology and structure of the nascent flare core can be shown by the shorter

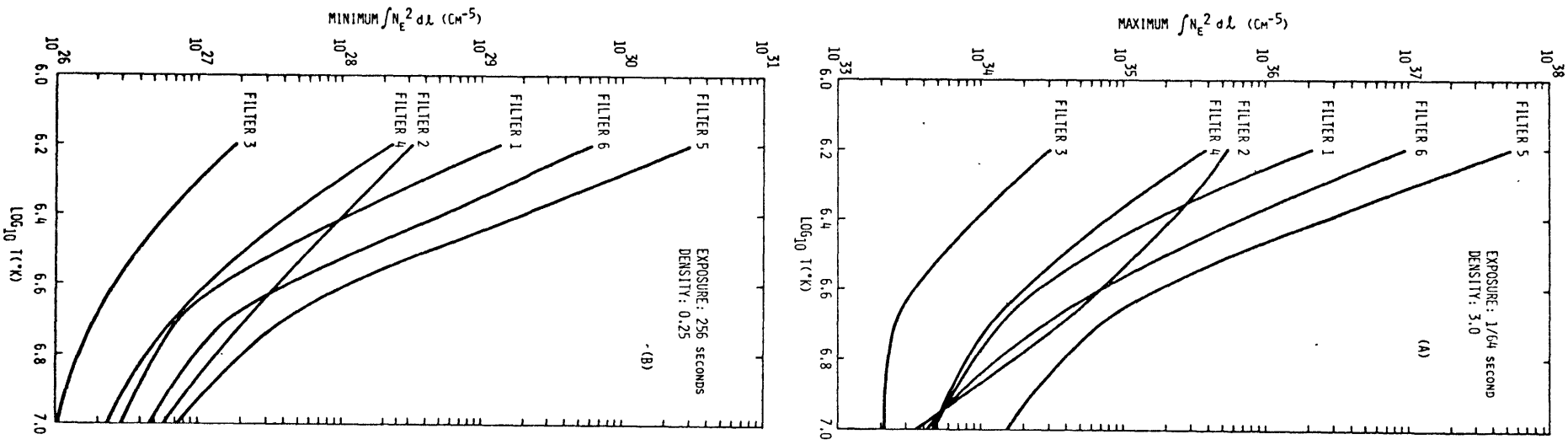

Figure 6 Emission integral as a function of temperature for brightest and faintest images

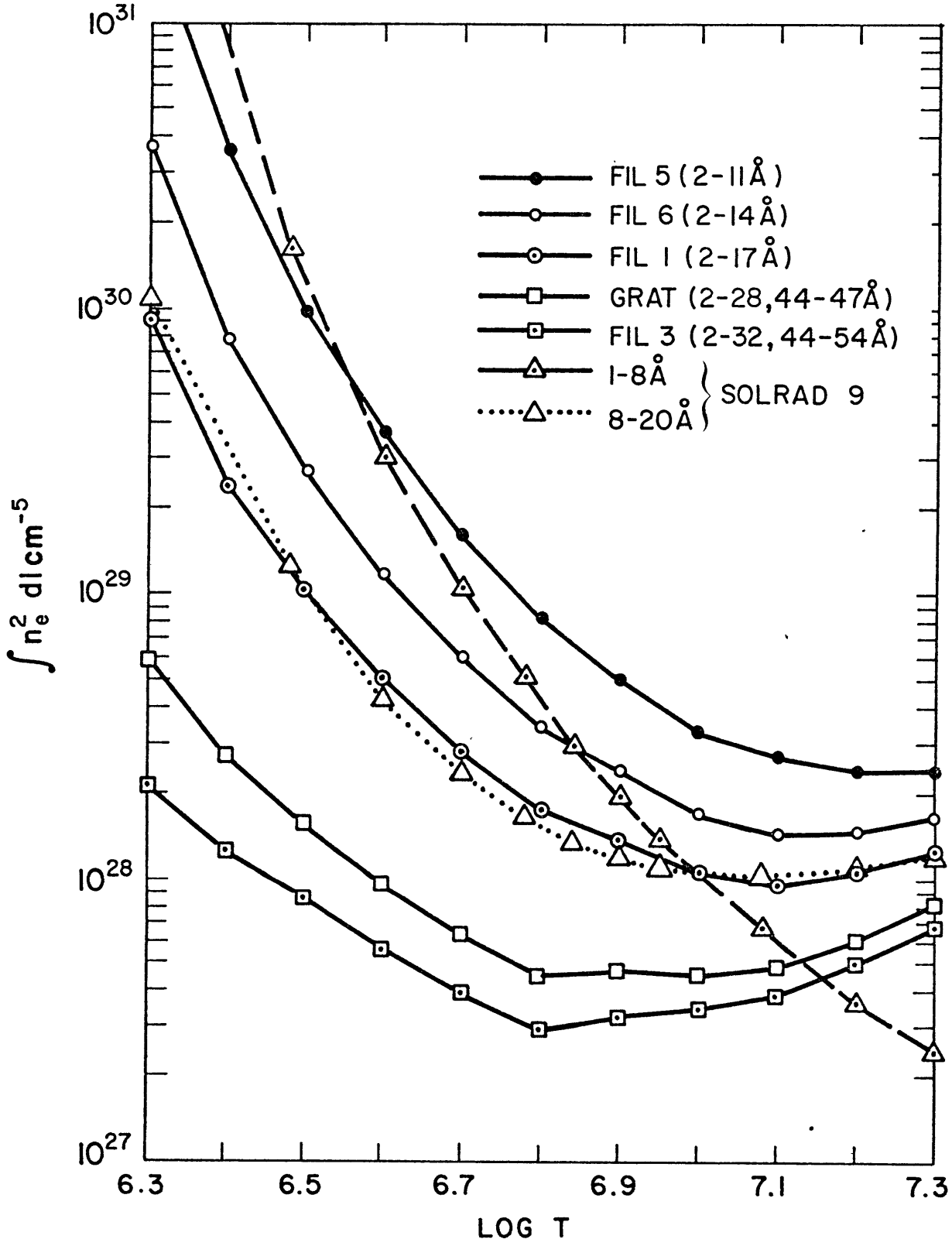
10^{31}
10^{30}
10^{29}
10^{28}
10^{27}
$\int n_e^2\, dl\, cm^{-5}$
6.3
6.5
6.7
6.9
7.1
7.3
LOG T
FIL 5 (2-11Å)
FIL 6 (2-14Å)
FIL 1 (2-17Å)
GRAT (2-28,44-47Å)
FIL 3 (2-32,44-54Å)
1-8Å
8-20Å
SOLRAD 9

FIG. 7

exposures, while longer exposures depict preexisting loops and other structures in the active region.

In this study, images on second generation film were used for a visual comparison to look for changes in X-ray morphology of the pre-flare active region. The photographic tolerances used in the second generation images and the sensitivity of the human eye to changes in intensity imply that changes of greater than 0.15 density units can be detected.[3] For our film and the telescope filters this corresponds to a temperature change of ~50% and an electron density change of ~25%. However, a structural rearrangement of unresolved features within the active region with no density or temperature changes may well go undetected in our analysis. An additional problem is that the telescope resolution grows worse with increasing distance from the telescope optical axis, so for several events changes in the telescope pointing between sequences of images make this comparison somewhat more difficult. This effect can be minimized by comparing other active regions before and after repointing.

FILM

The film used for the imaging was Kodak SO - 212, a panatomic emulsion imposed on a 0.0025 inch Estar base with antistatic backing. No gelatin topcoating was used since it would have attenuated the longer wavelengths. The film was stored in roll form in five magazines

each containing 1300 feet of 70 mm film or about 6500 images each. The shutters in the camera were able to allow for both white light (visible) and x-ray images. The white light images were included to facilitate alignment of the images and correlations with data from other sources.

THE PULSE HEIGHT ANALYZER

On board the SO - 54 instrument package was also a photoelectric x-ray detector consisting of a NaI scintillation photomultiplier covered by a 2 mil beryllium filter. The instrument recorded integrated solar disk flux and had a twofold purpose. First, it sorted the counts into 8 energy bins ranging from 10 keV to 80 keV with a pulse height analyzer(PHA). Second, it acted as a flare warning mechanism by representing the total flux as a number proportional to the log of the DC current of the monitor. An audio warning system is sounded and the astronaut can direct the telescope towards the flare and in addition use flare mode (short exposures) and the spectrograph. The position of the flare can be known by using a 7.6 cm diameter x-ray telescope with an image dissector. This particular use of the instrument assured the existence of many flare rises and decays in the data, but for the present study, the preflare times are too early for the instrument to have yet responded. Events are therefore only those which happened to be occurring when images were being taken.

The PHA was useful for acquiring onset and maximum times of flares and their profiles, particularly when the Solrad orbiting observatory was not in operation.

CHAPTER III - THE SOLAR FLARE

INTRODUCTION

Solar flares are outbursts of energy on the order of 10^{32} ergs which occur around magnetically active regions on the solar surface. They are accompanied by enhanced x-ray, thermal, radio, and cosmic ray emission as well as plasma ejection.

The flare phenomenon is an important one in astrophysics: it is the producer of the closest source of cosmic rays, and may give clues concerning the physical processes occuring in flare stars, a major class of variable stars. Solar flares are a testing ground for magnetohydrodynamic processes and the behavior of astrophysical plasmas.

The physical processes which cause flares are not as yet well understood. An understanding of the flare build-up process would be hastened by the existence of more observations of active regions during the preflare period.

THE FLARE EVENT

Solar flares are largely chromosperic phenomena reaching sometimes up into the corona proper. There seems to be quite a diversity among flares; some large H-α flares produce only small x-ray events, and some flares are primarily x-ray phenomena. There is also no

general correlation between radio events and solar flares, although although certain types of solar radio events are produced by the acceleration of plasma in solar magnetic fields during the flare event. Type III radio bursts are correlated with the impulsive hard x-ray bursts in the explosive phase of the flare, and acceleration of 10^{31} - 10^{33} electrons in the 0.1 - 3 MeV range accounts for type IV radio bursts in the decay phase.[4,5] See Appendix for descriptions of solar radio event types. Smith and Smith found no complete correlation between the impulsive acceleration of electrons and the optical flare,[6] but more recently, Vorpahl has suggested that the formation of H-α kernals, which are bright knots occurring on either side of magnetic neutral lines, is correlated with impulsive 8800 MHz microwave emission and hard x-ray spiked profiles.[7] Type II radio bursts, or nonthermal slow drift bursts, occur in the great solar flares.

There is no general correlation between particle and plasma emission and solar flares, but this phenomenon seems to be associated with the larger flares.

The flare covers an area on the order of 10^9 km^2; flares covering an area less than 3×10^8 km^2 are termed subflares. Until recently, with the advent of x-ray telescopes in earth orbit, most flare research was done in H-α. The Skylab x-ray telescope offers the first opportunity to study the solar x-ray flare extensively.

H-α flares are classified by their importance, which is determined by their area, on a scale of -1 (or s, for subflare), 1,2,3, and 4. In addition, the flare is assigned a letter, f (faint), n(normal), or b (brilliant), to describe its intensity.

Flares tend to be found near sunspots, more specifically in active regions with merging bipolar flux spots. The basic mechanism involved in the creation of the energy release is believed to be magnetic field line annihilation and reconnection. The largest flares begin by a brightening in knot - like areas on either side of the magnetic neutral line. The knots then form a strip. The early phase of the flare is often characterized by hard x-ray impulsive bursts, which account for the production of electrons in the explosive phase and spiked radio events, and are produced by bremstrahlung in a thermal plasma of $\sim 10^{10}$ e/cm^2.[8] Soft x-rays are produced by electrons in the 1 keV range and account for the bulk of the electron energy. Through the decay stage the flare is characterized by a progressively softer spectrum. Lower energy radiation tends to peak later in the event.

Magnetic fields in flares are not intense enough to suggest synchrotron radiation production by the harder x-rays.

Flares tend to take place in magnetically active regions. Although early studies had shown that the magnetic field simplified during a flare, and a reduction in field strength and an expansion of the

spot configuration occurred, Wiehr found that there was no change 1 hour after a flare of the magnetically complicated region,[9] and Janssens found no measurable change in the magnetic energy before and during a flare.[10]

No disturbances in the photosphere have been observed during the flare.[11]

ENERGY STORAGE AND RELEASE; THEORETICAL CONSIDERATIONS

The energy release in a typical flare is on the order of 10^{32} ergs. The source of this release is generally thought to be the conversion of magnetic energy to kinetic energy, specifically by the mechanism of magnetic field annihilation and reconnection. Any theory of flare development must take into account mechanisms responsible for both the general heating of the flare region, which is manifested in the optical (H - α) flare, and the existence of non-thermal x-rays and radio waves and particle streams, which are caused by the acceleration of charged particles. The magnetic field can simultaneously account for the existence of these two groups of phenomena; the first by the energy release in magnetic field annihilation, and the second by charged particle accelerations along the magnetic lines of force. In figure 8, it can be seen that magnetic field lines connect across the neutral sheet to form system B_1 or B_2. Hot plasma trapped under B_1 lines could account for thermal radio and x-radiation, and some of the

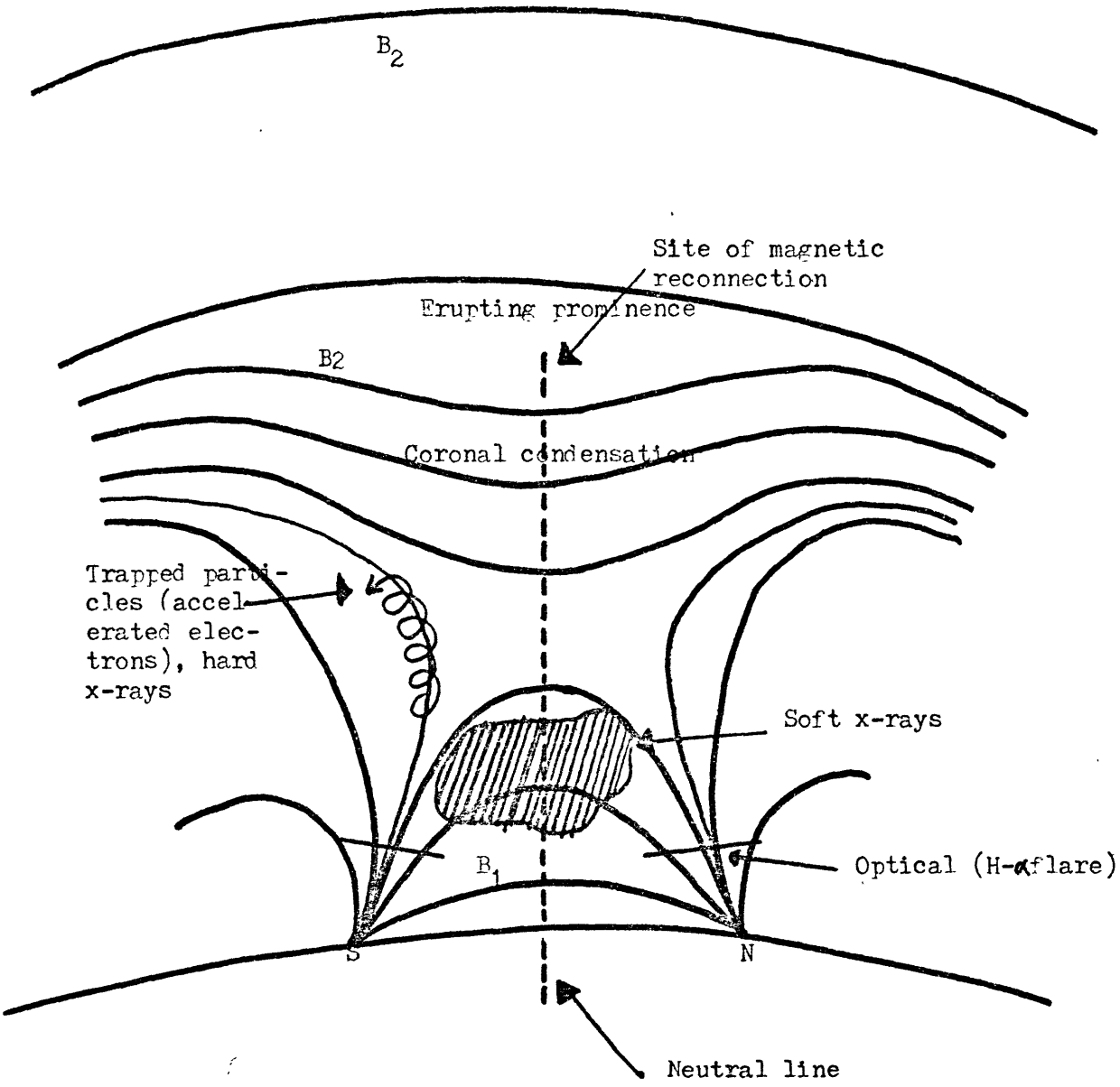

Figure Eight - The solar flare.

plasma is accelerated downwards by the Fermi acceleration mechanism in the magnetic "bottle" to cause the optical flare. Plasma moving upwards accounts for the eruptive prominences seen after some great flares. The level at which field lines reconnect determines the relative importance of the two motions and their associated phenomena.[12]

Several mechanisms have been proposed for the storage of the energy in the magnetic field, some relying on local storage mechanisms, others on more global mechanisms. Sweet gives a complete review of the possible processes.[11] Nonlocal sources evoke turbulent motions in the sun's convection zone. The theoretical response of the chromosheric plasma in such a case is consistent with observations. The mode of energy transport has been suggested to be high energy particles accelerated in subphotosheric magnetic fields.[13,14] Piddington[12] has suggested transport by hydrodynamic waves caused by subphotosperic turbulence and dissipation in the neutral atmosphere. Pneuman[15] hypothesized the energy to be the hydrodynamic (magnetoacoustic) flux normally heating the solar wind which is prevented from reaching the corona by the constraining magnetic fields.

Sturrock hypothesized that the energy in the closed field region is derived from photosheric motion and the energy stored in the upper open field region comes from the coronal nonthermal heating by the dissipation of hydrodynamic waves, which also drive the solar wind.[16]

More local sources of energy storage depend on magnetic energy stored by departure from a potential field. Sweet[17] and Parker[18] developed a mechanism in which two oppositely directed fields collide and interfere in times smaller than their characteristic diffusion times. Hydrodynamic turbulence can accelerate the process, but under certain conditions the turbulence can also amplify the magnetic field. A play-off between dissapative and amplifying forces exists with dissipation aided by decreasing the electric conductivity.[19]

Gold and Hoyle first suggested the existence of force-free twisted cylindrical flux tubes as a storage mechanism; the existence of vertical electric current near flare knots by Moreton & Severney is consistent with this mechanism.[20]

Sweet showed that gravitational and thermal energy stored in material above the magnetic field would not be sufficient to account for an energy storage mechanism.[11]

Several trigger mechanisms for the energy release have been proposed. In the Sturrock & Coppi mechanism, available gravitational energy triggers the release of magnetic energy.[21] Elliot described a process in which protons stored in the corona are released into the chromosphere when a local weakening of the magnetic field occurs.[14] Thermal instability is also a possible flare trigger mechanism. Parker and Field developed this model, which occurs at certain temperatures at constant pressure in which the rate of emission at thermodynamic

equilibrium decreases for increasing temperature.[22, 23]

Priest and Heyvaerts have made the suggestion that neutral sheets between new and old magnetic fluxes are thermally unstable and act as triggers.[29]

Field burst-through, in which the energy stored from the hydrodynamic waves usually heating and driving the solar wind breaks through, is produced in the models of Pneuman and Sturrock.

The release of the trigger mechanism marks the onset of the explosive phase of the solar flare. Unanswered questions include whether the acceleration of particles is a causal factor or a by-product of this phase, and whether the activity takes place in the chromosphere or the corona.

During the decay phase the energy is carried away by heat conduction and radiative cooling, mainly in the optical region. An unanswered question concerns how much matter is moved downward into the chromosphere to feed the optical flare. Both in the explosive and decay phase it is not certain whether turbulent heating or particle acceleration causes the radiation. A continued supply of fast electrons is needed to explain type IV radio bursts.

CHAPTER IV - OBSERVATIONS.

PREVIOUS WORK ON PREFLARE STUDIES

Martin and Ramsey studied 297 H-α flares for changes during the 2 hr. period prior to flare onset.[25] They discovered that in an H-α 0.5 A filter (which detects blue-shifted, rising features) a darkening filament could be observed in 53% of the flares. About 30 minutes before onset, a marked increase in pre-flare brightenings occurred.

DATA ANAIYSIS

The selection criteria for the flare events demanded that at least two images equivalent in time duration exist in the twenty minute time period preceeding flare onset. Onset was determined by profiles of full-scale flux measurements taken either on the SO - 54 pulse height analyzer or the Solrad 9 satellite's 8 - 20 ev or 1 - 8 ev ion chamber. The twenty minute period, which was later extended to 30 minutes to bring more events into the study, was chosen because the pre-flare events for the Marten - Ramsey study took place largely in this period. The flare profile with the two most common exposures, 64 and 256 seconds, is shown schematically in figure 9. The actual onset of the flare takes place before the apparent onset, since the detectors observe a background level which obfuscates the onset.

The other criteria for selecting the events were:

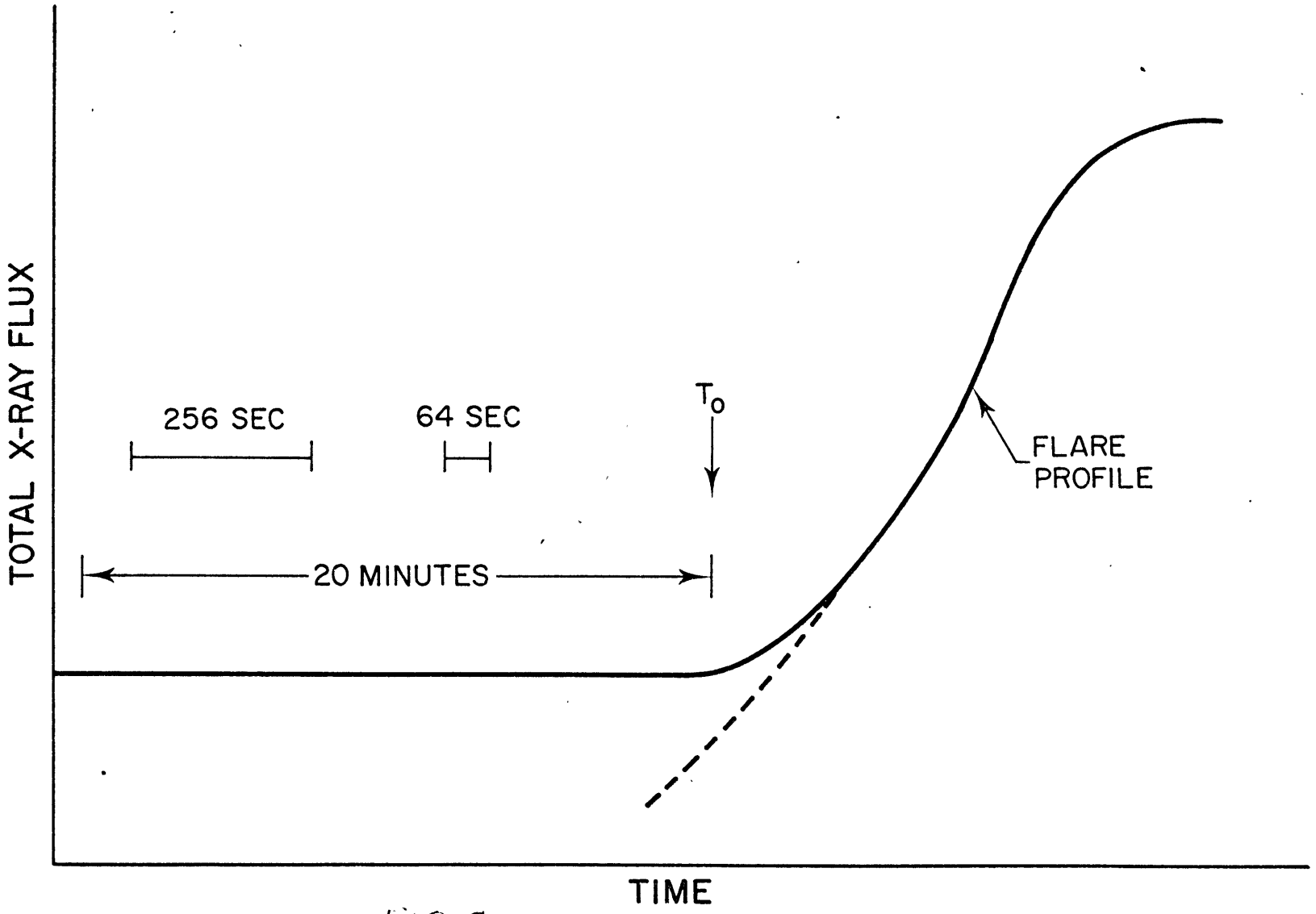
TOTAL X-RAY FLUX
256 SEC
64 SEC
T_o
20 MINUTES
FLARE
PROFILE
TIME

FIG. 9

1. The onset could be determined, i.e., the beginning of the flare profile existed in Solrad or the PHA output;
2. An x-ray image of the flare itself existed in order that any preflare phenomena could be correlated with the flare structure;
3. The flare was not at or near the limb of the sun, since limb flares would introduce geometrical effects. Such flares might, however, prove useful in determining the heights of preflare structures.

Ideally the exposures should also be in the same filter. However, with the relative filter responses shown in figure 7, it becomes legitimate to compare exposures from different filters if their responses are normalized. Filters with a similar response except for an additive constant, such as filters 5 and 6, and be easily interchanged for observations. The 19 events which follow the above criteria are listed in table I. The table lists the date of the event, the time of the onset, the time of maximum x-ray flux, the size of the flare as observed in the 1 - 8 Å band of the Solrad 9 ionization chamber, the reported H-α size, the time of H-α onset, the time and type of any associated radio events, and brief comments describing the x-ray onset.

Solrad size is determined as follows: Flares with a flux of 10^{-3} ergs/cm^2 in the 1 - 8 Å band are given a C designation, and M and X designations are given to 10^{-2} and 10^{-1} flares, respectively.

Finer classification is accomplished by assigning the numerals 1 through 9.

Second generation positive images made directly from the negative flight film were used to visually detect morphological changes in the x-ray active region prior to flare onset. As stated in the instrumentation chapter, a limit of 0.15 density units change is set by the sensitivity of the human eye and the photographic tolerences in second generation film. This density change corresponds to a temperature change of 50% and an electron density change of 25%.

The film used in this survey study is capable of being subjected to much more rigorous analysis. Quantitative descriptions can be acquired by subjecting the film to densitometer measurements. By means of a density to energy conversion, the density units registered on the film can be expressed equivalently as the total energy of the photons striking the surface of the film.

To produce a density to energy conversion, a laboratory calibration of the film's sensitivity to a source of known energy and flux is required. Such a calibration was carried out for the SO - 54 experiment using an 8.2 $\mathring{A}$ x-ray source which approximated the energy spectrum of the incident photons onto the film in the actual experiment. Several strips of film were subjected to successively longer periods of exposure. The strips of film, which comprised a stepwedge, were then measured on a McMath densitometer. Since the density measurements of each wedge correspond to a known energy flux, a plot of density versus energy can be constructed. This plot forms the basis for converting

measured density units in a particular image to an equivalent energy flux array. The density to energy conversion can be used successfully only in the region where the response of the film is linear. At high and low densities the plot forms a "toe" and "shoulder" region, where the film is, in effect, undersaturated and oversaturated. Time evolution of a particular area of an active region on a density or energy array can be seen by comparing successive images of equivalent filters and exposures. As in all densitometry work, care must be taken to subtract out "fog" or background counts.

For a survey study such as the present one, this detailed analysis on individual flares was not done. Further work in this area, including estimates of the evolution of electron temperatures from how hard the spectrum is as evidenced by relative transmissions through the several filters, is possible.

THE EVENTS

The observations of the preflare periods are summarized in Table I. The September 2 16:17 event was preceeded by another flare approximately 15 minutes before the onset, but this flare is presumed not to be directly related to the flare under study. The flares of August 7 and September 3 were also preceeded by the decay of previous flares.

All times are expressed in Universal Time (UT).

Table I The Preflare Periods

Event time	Onset (UT)	Maximum	Solrad Size	Active Region	H-α Size	H-α Onset
June 15, 1973	14:00	14:18	M2	993	1B	14:19
June 15, 1973	22:01	22:08	C1	382	-B	22:00
Aug. 7, 1973	18:36 20:17	18:47 20:20	C5 <C	474	-N --F	18:37 20:21
Aug. 9, 1973	15:47	15:50	M2	474	--N	15:51
Aug. 31, 1973	20:48	20:50	<C.4	507	---	---
Aug. 31, 1973	23:57	23:58	C1	511	-F	23:57
Sept. 1, 1973	18:22	18:28	C2	507	--F	18:25
Sept. 1, 1973	23:04	23:15	C1	512	-N	22:57
Sept. 2, 1973	00:42	00:45	C4	512	-B	C0:42
Sept. 2, 1973	16:17	16:20	C2	512	--F	16:25

Radio event type and time		Comments
45;20	14:11.5;14:16	Two large loop structures brighten. Flare volume is about half of the preflare brightened volume. See plate I.
none		Consolidation of looplike flare core 2 minutes before onset.
1; 1,3	18:16; 18:40-18:47	Previous C3 flare decays. A kernel brightens during the 5 minute period preceding the flare. The kernel and an adjacent small loop are the site of the flare. See plate II.
1	15:44.4	Takes place in a kernel pre-existing for 5 hours.
none		No preflare changes.
none		No change apparent until 1-2 minutes before the flare onset.
22	18:18.7	No changes.
20	22:55onset 23:25 max	Kernel brightens and dims, then a more extended region ~20" distant from the kernel flares.
1	00:42	No changes in kernel which forms flare core.
none		A C2.5 flare occurs at 16:02, then the active region returns to its preflare state. No change is obvious in preflare image at 16:17, so time scale for change must be ~1 min.

The Preflare Periods, continued

Event time	Onset (UT)	Maximum	Solrad Size	Active Region	H-α size	H-α onset
Sept. 3, 1973	23:14	23:19	C.8	510	-N	23:35 (probably too late)
Sept. 4, 1973	00:50		C2	510	-N	00:52E
Sept. 4, 1973	16:32	16:40	C7	510	-N	16:27
Sept. 5, 1973	18:28	18:32	M2	510		
Sept. 6, 1973	01:05	01:10	C2	510	--F	01:06
Sept. 6, 1973	16:25	16:28	C3	507	-N	16:16
Sept. 6, 1973	18:14	18:25	~C2	512	--B	18:13
Sept. 7, 1973	~16:02	~16:08		513	-F	16:02
Jan. 19, 1974	18:41	18:42	C1	708	--F	18:40

Radio event type and time		Comments
45	23:21	A small subflare decays away. A faint loop forms and is first easily seen about 8 minutes before onset. A kernel also forms, but the resulting flare occurs in the region of the previous subflare. See plate III.
45	00:51.5	No change.
1	16:27.5	Gap in data; no changes up to 10 minutes before the onset.
1,3	18:28.5	The loop forming the core appears less than 2 minutes before onset.
45;1	03:03	Brightening and dimming of a loop 5 minutes before onset.
1	16:25.5	Brightening and dimming of a loop 14 minutes before onset.
3;22	18:18	A slight enhancement of a northern loop may have begun about 18:05. No enhancement of the brightest flare loop could be seen as late as 18:10. See plate IV.
1,3	16:05	No changes.
1	18:26	A small loop and a large diffuse region begin to brighten about 5 minutes before the onset. The flare forms in a second small loop 10 arc sec to the west of the first loop. See plate V.

In the following section several of the more interesting flares are discussed in detail, with correlations with H-α events, radio events, and magnetograms, if available. Studying the magnetic field immediately prior to flare onset presents a problem because magnetograms are taken at only a few observatories, and only at 6 - hour intervals. Mt. Palomar Observatory magnetograms of the longitudinal magnetic field were used. H -α images taken at Sacramento Peak Observatory were provided by David Rust of American Science and Engineering. The National Oceanic and Atmospheric Administration's monthly compendium of solar and geophysical data was used to search for associated radio events, and to get additional data on the H-α and x-ray flare events, such as intensities, profiles and onsets. Hirman et. al. also published a list of solar flares detected during the Skylab mission.[29]

The H-α images from Sacramento Peak were taken at 5 second intervals. Offband H-α images, which show the hottest features, were taken intermittently.

A NOTE ON ALIGNMENT

For rigorous correlations between morphological structures of the H -α and x-ray images, accurate alignmentments of the two images must be made. First, the Sacramento Peak H-α images were blown up to the size of the Skylab x-ray images (11.5 cm diameter) and the available magnetograms were reduced to the same size. A

Stoneyhurst disk, which is a grid of solar latitude for a particular latitude and longitude for a particular time of year, is superimposed on the solar x-ray image after marking solar north, which is available from data taken onboard Skylab. The H-α image or magnetogram, marked with solar north, is then superimposed on the image and grid. Correlation is made with both markings of solar north, and with all active regions appearing on the solar disk in the images.

THE FLARE OF JUNE 15 22:01

A C1 flare with a reported -B H-α flare which peaked at 22:05, approximately 3 minutes before the x-ray peak, was characterized during the preflare period by the consolidation of a looplike structure 2 minutes before flare onset. This loop became the site of the flare core. The profile of this flare lacked an impulsive phase (spiked profile in the higher energy x-ray bands), and no radio events were reported.

THE EVENT OF JUNE 15 14:00

26

This event is shown in plate 1. Two preflare images are shown. In B two large loop structures indicated by arrows showed a distinct brightening during the 6 minute interval between A and B. Images during the flare rise are shown in C and D. The brightest part of the flare is composed of a volume which is substantially smaller that the region which was enhanced in the preflare period.

The impulsive radio event at 14:11 occurs during the rise phase.

THE FIARE OF AUGUST 7 18:35; 20:20

This event is shown in plate II. The image at 18:15 was taken during the rise phase of a subflare. By 18:29 the two eastern regions which flared have dimmed. Several minutes before the flare onset a small kernal designated by the arrow begins to brighten. It is joined by a second kernal, which can be resolved into a loop, shown in the image at 18:37. After these features had attained flare brightness a second larger region indicated by the arrow at 18:46 became the brightest part of the flare. This latter feature showed no enhancement prior to the flare onset other than that which occurred in the earlier flare at 18:15. In this event, a part of the flaring region was observed to brighten early, but only by several minutes prior to the onset.

The H-α images from Sacramento peak were somewhat obscured by fog, but a definite brightening in the area of the northern kernal, the site of the previous flare and the latter part of this flare, can be discerned in H-α. The whole scheme is shown in figure 10, along with magnetogram data. The x-ray kernals appear near a neutral line.

Radio events can be correlated with the kernal brightenings. For the 18:15:30 kernal brightening an impulsive type I event occurs at

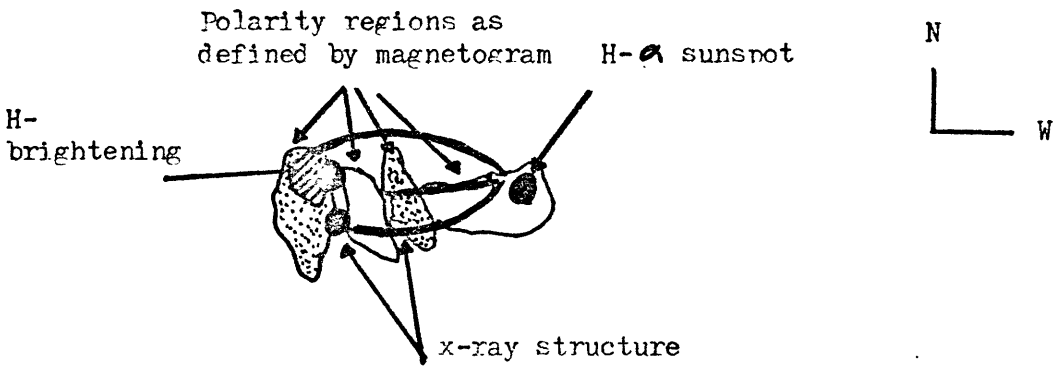

FIGURE 10 THE EVENT OF AUGUST 7

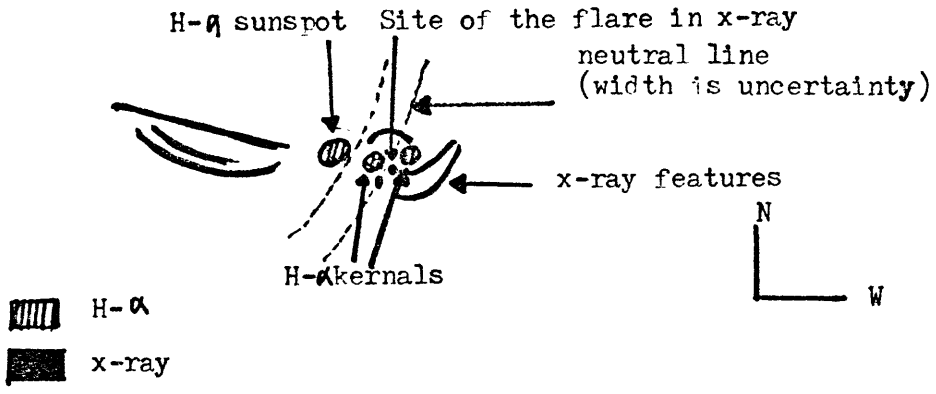

FIGURE 11 THE EVENT OF SEPTEMBER 3

18:16 and for the 18:35 kernal brightening, many impulsive events occur from 18:40 - 18:47.

At 20:17 a <C flare takes place 0.2 arc minutes east of the previous flare, at the tip of the northwest loop. This flare was not characterized by any preflare brightenings, and no impulsive radio events were reported. A --F flare was reported at 20:21 onset.

THE AUGUST 9 EVENT

This event occurs in a kernal which had preexisted for at least five hours. No pre-flare brightening outside the kernal took place. At 15:44, two minutes after the x-ray onset, a series of impulsive type I radio events with a 5 FU peak occur. A --N H-α flare starts at 15:51 and peaks 2 minutes later.

THE EVENT OF SEPTEMBER 1 23:04

Approximately 6 minutes before the onset of the flare a sharp kernal appears and brightens; 3 minutes later it dims. The onset of the flare takes place in a more diffuse area of the active region about one arc minute east of the kernal. The kernal again brightens at 23:11 to form part of the flare structure, but this time it is a pair of kernals separated by about 0.4 arc seconds.

An H-α -N flare started at 22:27. The Sacramento Peak images show the position to be correlated with the x-ray flare, but the brightenings occur about five minutes later. A type 20 (nonimpulsive) radio event starts

at 22:55 and peaks at 23:25.

THE EVENT OF SEPTEMBER 2 00:42

This event occurs in an x-ray kernal which shows no change prior to onset, at which point it sharpens and consolidates. There are two other faint kernals in active region 507, one brighter than the flare kernal; neither of these kernals show changes. Both an H-α -B flare and an impulsive type I radio event occur at 00:42, one minute before the x-ray onset.

THE EVENT OF SEPTEMBER 2 16:18

A previous C2.5 flare occurs at 16:02, then the active region returns to its preflare state. No change occurs in the active region up to one minute prior to onset at 16:17, at which time a kernal forms the flare core. There were no reported radio events and an H-α--F flare at 16:25.

THE EVENT OF SEPTEMBER 3

Images from three different passbands are shown in plate III. This preflare period was one of the most complex of the events. A small flare can be seen in the first three images from 22:54 to 22:59. The region then becomes dim but a very faint loop appears which is indicated by the arrow at 23:06. The kernal (indicated by an arrow) also brightens

at 23:09. The principal flare structure begins to brighten at 23:11 and can be seen in the flare state at 23:13 and 23:19. If the kernal and loop structure took part in the flare, they were only minor components of the event.

In figure 11 is shown a diagram superimposing the x-ray features with H-α features. The x-ray kernals appeared adjacent to two H-α kernals, which were originally described by Vorpahl[7] and found to be associated with impulsive microwave bursts and hard x-ray spikes. Vorpahl found that they appear on either side of a neutral line. The position of the neutral line is drawn in the diagram, with its thickness representing the uncertainty in its position due to alignment inaccuracies.

The H-α kernals appear in off-band H-α images and reach a maximum at 23:28. A surge starts at 23:32. A type 45 radio burst at 23:21 with 210 FU maximum and 1.5 minutes duration occurred. This does not correlate with the original kernal brightening.

THE EVENT OF SEPTEMBER 4 16:32

This C7 flare was unfortunately preceeded by a 10 minute gap in the imaging; up until the gap no changes occurred in the active region. The site of the flare is a kernal, and the hard x-ray onset is accompanied by a -N H-α flare and type I radio events.

THE EVENT OF SEPTEMBER 5 18:28

The event is a large (M2) impulsive flare whose core is a loop about 0.44 arc minutes across. This loop does not appear until less than two minutes before flare onset. The loop, and two disconnected kernals appear as part of a group of preexisting x-ray kernals situated around an H-α sunspot (see figure 12). H-α kernals, which are the predominant feature in off-band H-α, appear at the foot points of this loop. The timing of their appearance is uncertain because of an error in the recorded times on the Sacramento Peak H-α films and a hiatus in flare patrol from 18:18 - 18:28, but it was sometime between 18:28 and 18:30. The western kernal moves towards the sunspot as the flare approaches maximum, and is the source of an ensuing surge. A series of impulsive radio events starts at 18:26.4. This correlates well with the formation of the loop core between 18:26.5 and 18:27.5.

The magnetogram shows that the sunspot is embedded in a region of polarity opposite from that of the surrounding kernals. The flare appears to take place in a "kink" in the neutral line.

THE SEPTEMBER 6 01:05 EVENT

The pre-flare period of this C2 event is characterized by a brightening and dimming of a loop which later forms the flare core. Five minutes before onset, the loop, which is about 0.2 arc minutes

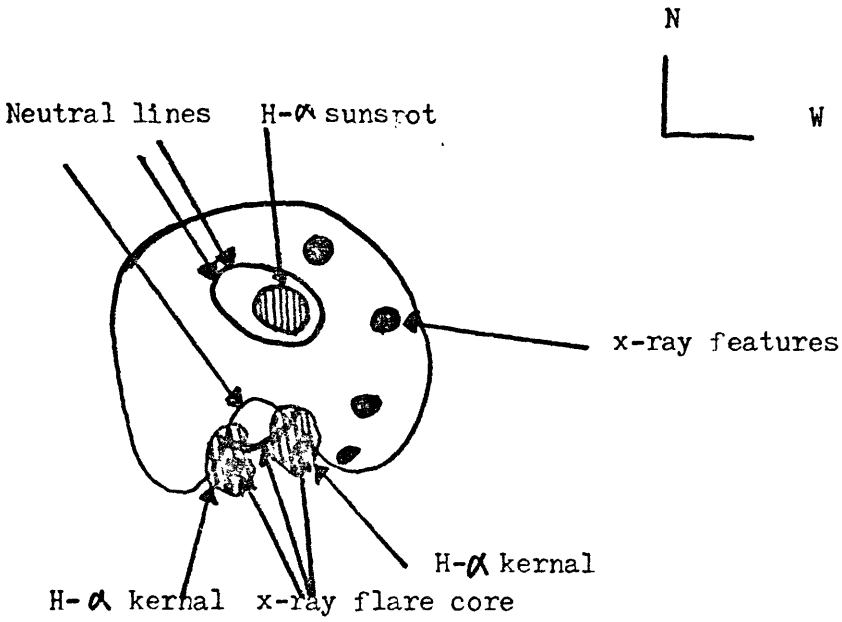

FIGURE 12 SCHEMATIC REPRESENTATION OF THE SEPTEMBER 5 18:28 EVENT

across, brightens. Two minutes before onset it dims. Two longer adjacent loops one arc minute across and approximately 0.5 arc minutes away remain unchanged. A type I radio event starts at 01:03 and a --F H-α flare begins at 01:06. It is possible that there is a connecting loop from outside active region 510.

THE SEPTEMBER 6 16:25 EVENT

Fourteen minutes before onset, two newly existing linear structures consolidate and form a loop about 0.5 arc minutes across. Three kernals appear along the structure, one of which brightens 12 minutes before onset. Seven minutes before onset, the linear structure with the brightened kernal is not visible. At onset, both structures appear and continue to brighten. A Type I radio event occurs at 16:25.5, close to the 16:25:50 onset which appears in the x-ray images. The H-α -N flare starts at 16:16 and peaks at 16:25, which would put it in the time period of the pre-flare brightenings.

THE EVENT OF SEPTEMBER 6 18:14

Images from three different passbands are shown in plate IV. A faint loop in the northern part of the active region (indicated by an arrow) shows a slight enhancement starting at 18:08 or earlier. However, the brightest structures seen in the flare onset at 18:17, in particular the southern loop indicated by the arrow, showed no preflare enhancement as late as 18:10, less than

7 minutes prior to the flare onset.

A type III radio event starts at 18:18, reaches maximum at 18:19.5 and lasts five minutes. The loop comprising the flare core forms between 18:10 and 18:17, before the onset of this radio event. An H-α --B flare begins at 18:16 and a check with the Sacramento Peak images shows that the bright flare region coincides with the northern top of the southern loop.

THE EVENT OF SEPTEMBER 7 16:08

This event is characterized by a lack of pre-flare changes. The flare occurs in the footpoint of a 1.7 arc minute loop which forms at onset. This loop is next to a similar but larger preexisting loop. On the Sacramento Peak films, there appears a sunspot at the western footpoint of the loop. The H-α brightening appears as two patches near the foot points of the loop. A type I radio event began at 16:05, but this event may be associated with another flare on the limb.

The onset of this flare is uncertain because the Solrad profile may represent the limb flare.

THE EVENT OF JANUARY 19

This event was observed in a high data taking mode, some images of which are shown in plate V. A telescope repointing occurred between

the images at 18:27 and 18:31, and no morphological change can be associated with those two images. The first brightening occurred at 18:39 and consisted of a small loop ~15" in length and the region surrounding the loop. Only 13 seconds separate the two bottom left images of plate V, but during this time a second loop (shown by arrow) about 10" west of the first loop also appeared. The overexposed image at 18:42 shows a strut pattern which can be used to find the center of the flare emission. We found that the center of flare emission was coincident with the second loop structure to within an uncertainty of ~ 3". Furthermore, the strut pattern indicates that the size of the flaring structure was comparable to the size of the loop shown at 18:40. The structure which brightened in the preflare was not a major contributor to the subsequent flare.

OTHER EVENTS

A small (< C.4) event on August 31 at 20:48 exhibits no preflare changes. A loop brightens at onset. There is no H-α or radio event.

Another August 31 event at 23:56 shows no changes until 1-2 minutes before onset. The quality of the images is poor, but the brightening appears to be a kernal. There were no radio events, and a -- F H-α flare started at 23:57.

A September 1 C2 event at 18:28 exhibits no change except a consolidation of the loop which brightens at onset and forms the flare structure. A --F H-α flare began at 18:25.

A small (< C1) flare on September 4 occurs in a group of x-ray kernals surrounding a sunspot. The flare core, which is a loop and a smaller bright area, shows no preflare changes. The flare occurs near the neutral line separating the polarities of the kernals and the sunspot. A type 45 radio event occurs at 00:51.5.

CHAPTER V - SUMMARY AND CONCLUSIONS

The events can be summarized as follows:

1. Preflare brightening- larger area than flare core		June 15 14:00
2. Preflare brightening in another part of active region		Sept. 3 23:14 Sept. 6 18:14 Jan. 19 18:41
3. Preflare brightening in part of flare core		Aug. 7 18:36
4. Brightening in flare core		Aug. 31 23:57 (t~1 min) June 15 22:05 (t~2 min) Sept. 5 18:28 (t<2 min)
5. No change.	Aug. 9 15:47 Aug. 31 20:48 Sept. 1 18:28 Sept. 2 00:42	Sept. 2 16:17 (t 1 min) Sept. 4 00:50 Sept. 4 16:32 Sept. 7 16:02
6. Brightening, then dimming of flare core		Sept. 6 01:05 Sept. 6 16:25
7. Preflare brightening, then dimming in another part of active region		Sept. 1 23:04

Two points figure in the 19 preflare periods observed: there is a lack of uniformity in the morphological changes and brightenings, and a large number of flares (8) exhibited no preflare changes up to a few minutes before onset of the explosive phase of the x-ray flare. For events in which only the flare core itself brightened

in the preflare period, the changes were either seen less than two minutes before onset, or the region subsequently dimmed before onset. There was no flare which exhibited a gradual build up in the flare core. The September 6 16:25 event came closest to this situation, but the core dimmed again before onset. The H-α flare for this event started earlier than the x-ray event by about 10 minutes.

The three events which showed some type of brightening and dimming before onset may suggest that a precursor event exists for at least some solar flares.

Another important result from the data is that adjacent areas of the active regions are as likely to contribute to morphological changes prior to the flare onset as the core itself.

Vorpahl et. al. observed that on a soft x-ray telescope the flare core could be seen in the longer exposures before the onset of the flare.[27] A gradual heating and storage mechanism was implied. In this study, a sudden increase in x-ray energy proved to be the more general case.

The formation of kernals and small loops, sometimes accompanied by impulsive radio events, was characteristic of the rise phase, not of the preflare phase. The H-α kernals described by Vorpahl[7] were seen to exist at the footpoints of such loops or adjacent to the kernals.

In an event like September 1 23:14, the brightening of kernals

before flare onset might suggest non - thermal acceleration of hard electrons as a precursor and energy source for the flare. But this scenario was not observed in a general way. In addition, this particular kernal was not correlated with the impulsive radio events associated with acceleration of hard electrons.

The preflare observations were not determined by the size or type of the flare. For example, large flares did not show more substantive energy storage than smaller flares.

The fact that other parts of the active region contributed to the preflare period may lead to better estimations of the size scale of flares and sites of preflare energy storage and sources of plasma injection. However, the possibility still exists that non flare core changes are not related to the flare event. A more extensive study of detailed activity in x-ray active regions would have to be carried out to evaluate this problem. Further study should also lead in the direction of surveying more events, although this may have to wait for new experiments because this work represents a thorough survey of the Skylab S-054 data.

APPENDIX

The key for identifying type of solar x-ray event is as below:[28]

1 = Simple 1
2 = Simple 1F
3 = Simple 2
4 = Simple 2F
5 = Simple
6 = Minor
7 = Minor +
8 = Spike
20 = Simple 3
21 = Simple 3A
22 = Simple 3F
23 = Simple 3AF
24 = Rise
25 = Rise A
26 = Fall
27 = Rise and Fall
28 = Precursor
29 = Post Burst Increase
30 = Post Burst Increase A
31 = Post Burst Decrease
32 = Absorption
40 = Fluctuations
41 = Group of Bursts
42 = Series of Bursts
43 = Onset of Noise Storm
44 = Noise Storm in Progress
45 = Complex
46 = Complex F
47 = Great Burst
48 = Major
49 = Major +

EXAMPLES OF SOLAR RADIO EVENTS (Pennsylvania State University)

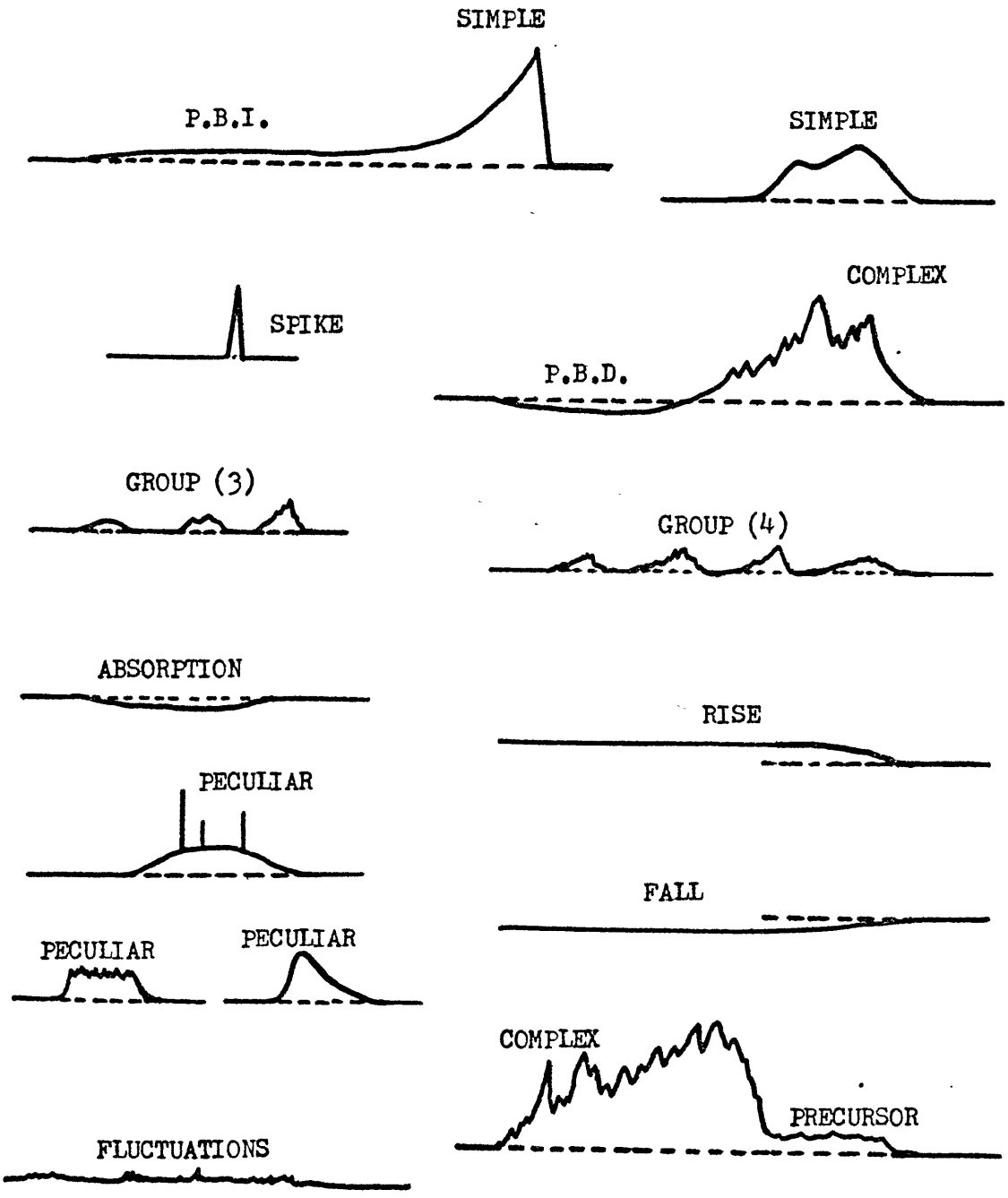

Note: Time increases from right to left on all figures.

REFERENCES

1. Vaiana, G. S., Krieger, A. S., Petrasso, R., Silk, J. K., Timothy, A. F. 1974, Proc. Soc. Photo-optical Instrumentation Engineers 44.

2. Giacconi, R., Rossi, B. 1960, J. Geophys. Res. 65, 773.

3. Kahler, S., Buratti, B. 1976, Proc. Flare Build-up Conference.

4. Takakura, T. 1967, Solar Phys. 1, 303.

5. Kane, S. R. 1972, Solar Phys. 27, 174.

6. Smith, H. J., Smith, E. P. 1963, Solar Flares, 199.

7. Vorpahl, J. A. 1972, Solar Phys. 26, 397.

8. Arnoldy, R. L., Kane, S. R., Winckler, J. R. 1968, Proc. IAU Symp. 35, 490.

9. Wiehr, S. 1972, Solar Phys. 26, 250.

10. Janssens, T. J. 1972, Solar Phys. 27, 149.

11. Sweet, P. A. 1969, Ann. Rev. Astron. Astrophys. 8, 149.

12. Piddington, J. H. 1969, Cosmic Electrodynamics, 74.

13. Warwick, T. W. 1962, P.A.S.P. 74, 302.

14. Elliot, H. 1968, Proc. XI COSPAR Symp. Solar Flares.

15. Pneuman, G. W. 1968, Solar Phys. 2, 462.

16. Sturrock, P. A., Proc. IAU Symp. 35, 471.

17. Sweet, P. A. 1958, Proc. IAU Symp. 6, 123.

18. Parker, E. N. 1963, Ap. J. Suppl. 8, 77, 177.

19. Tandberg-Hanssen, E. 1967, Solar Activity, 292.

20. Moreton, G. E., Severny, A. B. 1968, Solar Phys. 3, 282.

21. Sturrock, P. A., Coppi, B. A. 1966, Ap. J. 143, 3.

22. Parker, E. N. 1953, Ap. J. 117, 431.

23. Field, G. B. 1965, Ap. J. 142, 531.

24. Priest, E. R., Hayvaerts, J. 1974, Solar Phys. 36, 433.

25. Martin, S. F., Ramsey, H. E. 1972, Prog. in Astronautics and Aeronautics 30, 371.

26. Pallavicini, R., Vaiana, G. S., Kahler, S. W., Krieger, A. S. 1975, Solar Phys. 45, 411.

27. Vorpahl, J. A., Gibson, E. G., Landecker, P. B., McKenzie, D. C., Underwood, J. H. 1975, Solar Phys. 45, 199.

28. N.O.A.A. Feb., 1972, Solar and Geophysical data, 45.

29. Hirman, J., Iosey, R., amd Heckman, G.1975, "A Compilation of Solar flares Reported during the Skylab Mission - Preliminary copy."

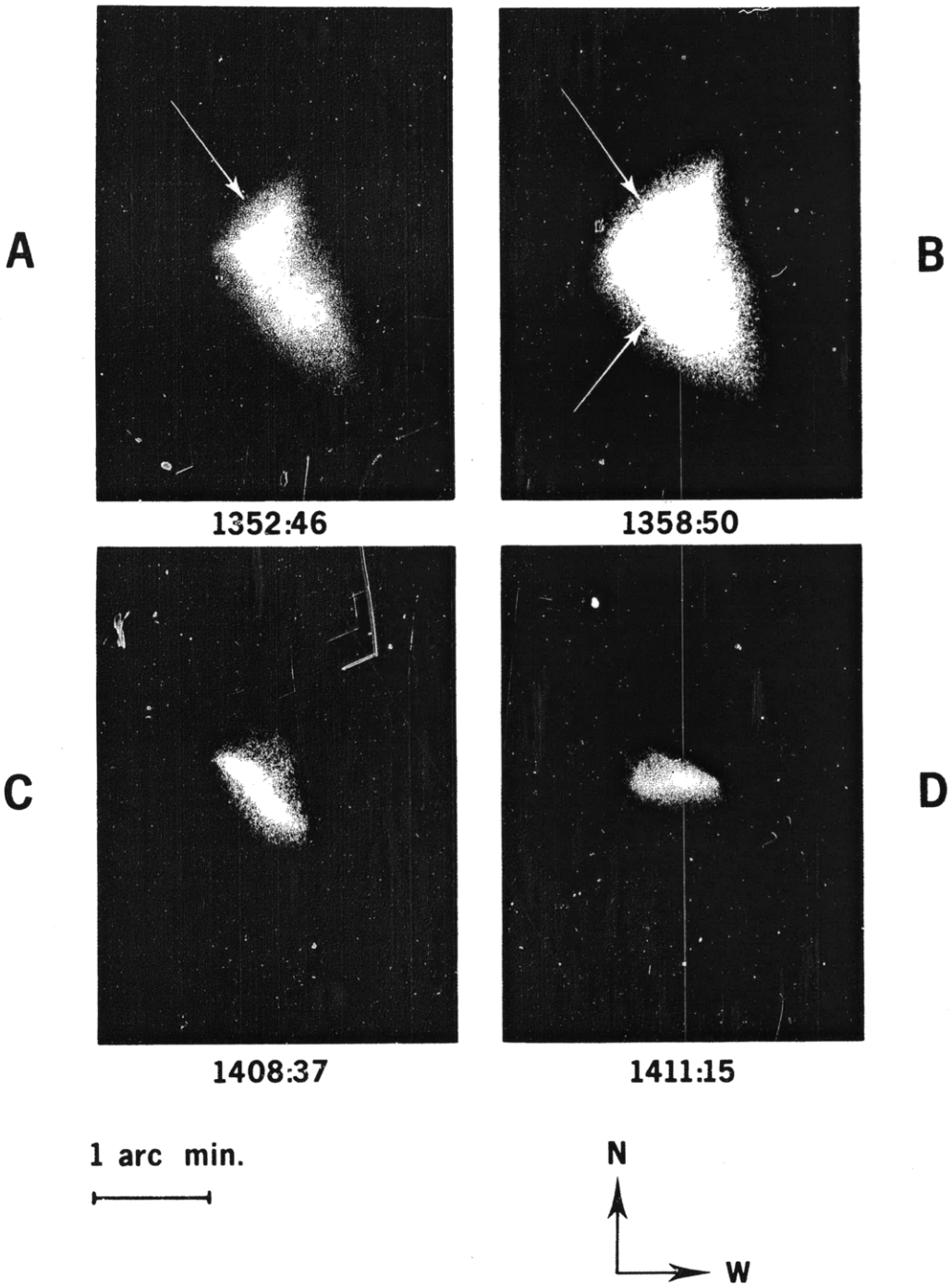
A
B
1352:46
1358:50
C
D
1408:37
1411:15
1 arc min.
N
W

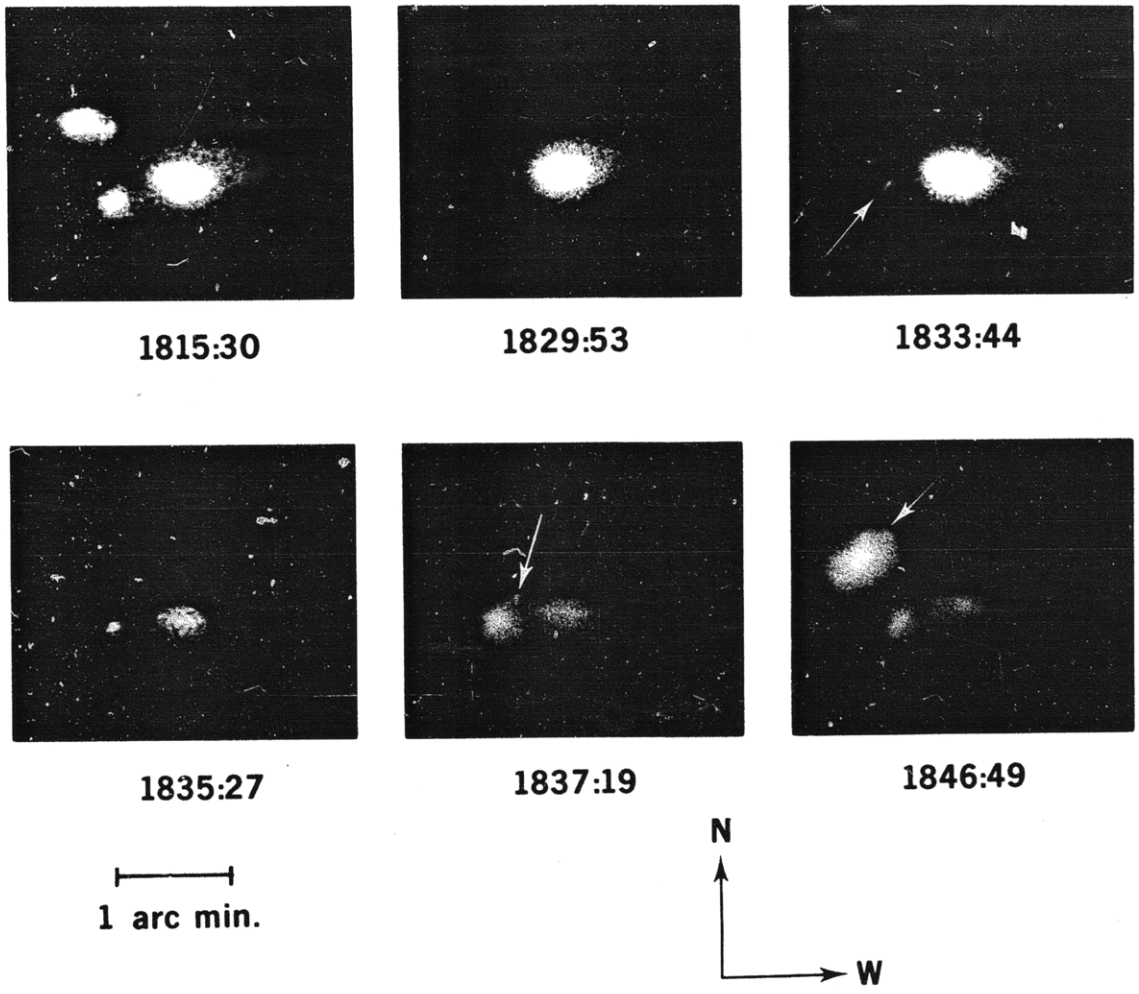

AR 474 AUGUST 7, 1973 S-054

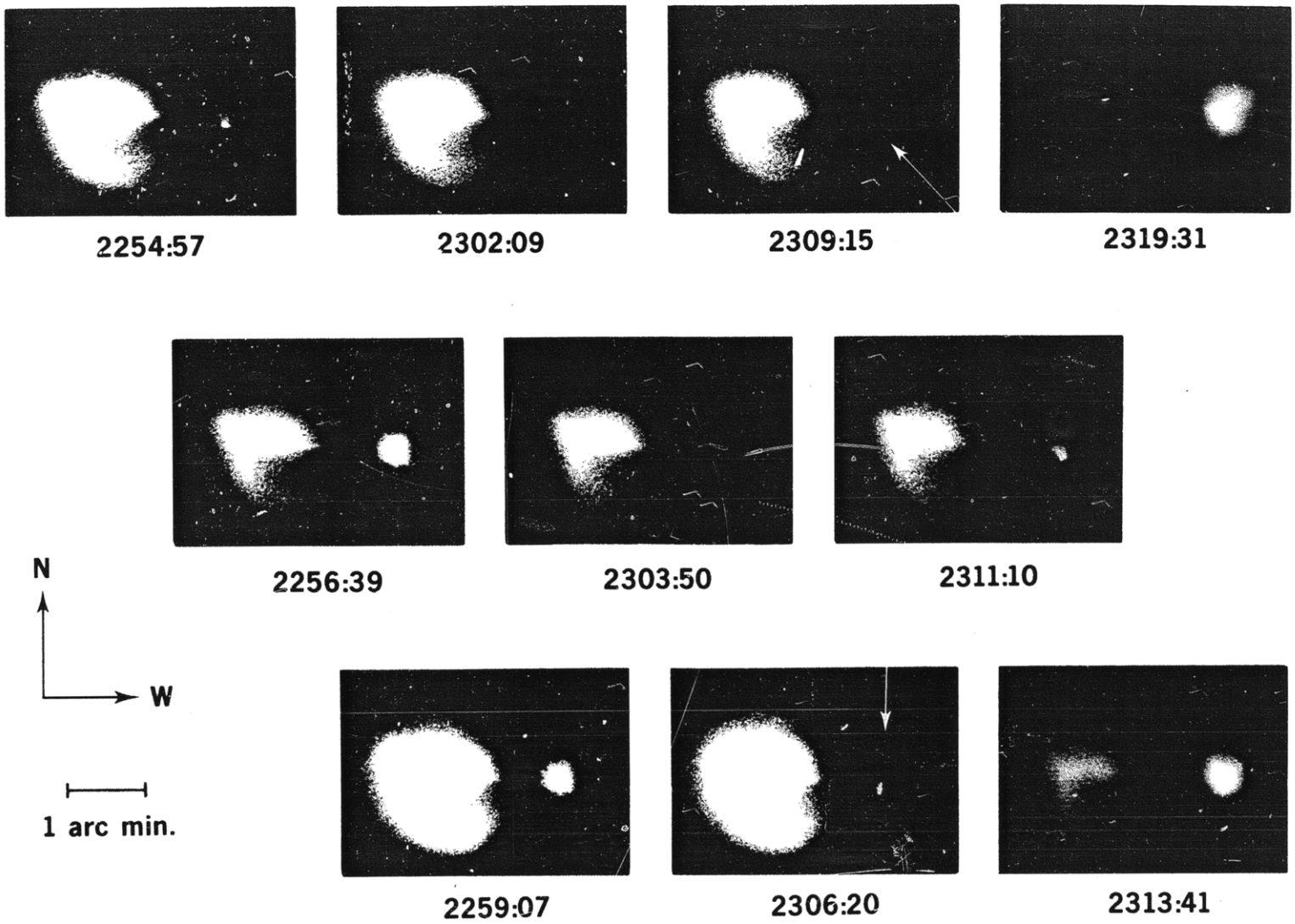

AR 510 SEPTEMBER 3, 1973 S-054

1756:01

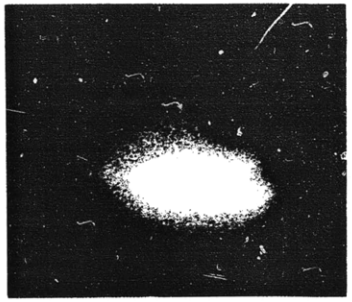

1805:04

1815:53

1801:20

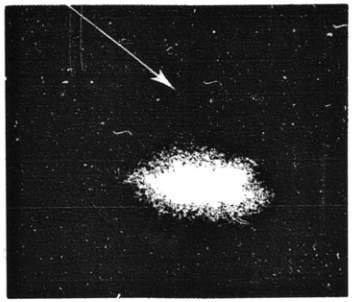

1808:42

1817:27

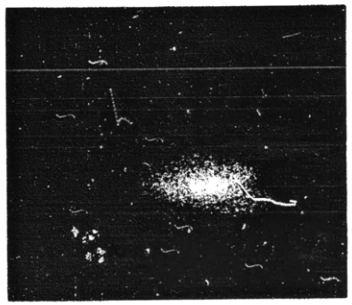

1802:53

1810:39

AR 512 SEPTEMBER 6, 1973 S-054

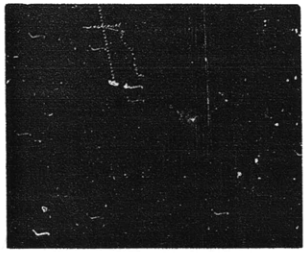

1821:34

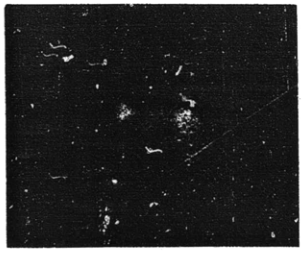

1824:23

1827:12

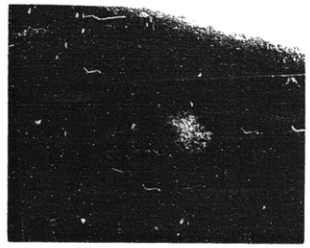

1831:25

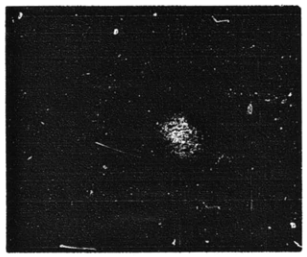

1834:02

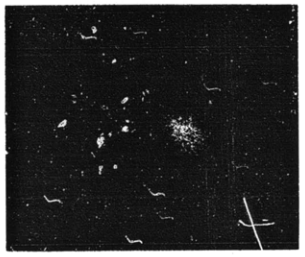

1836:51

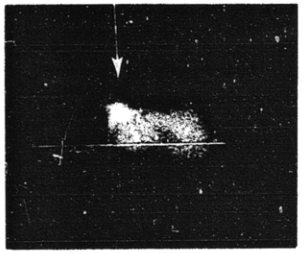

1839:28

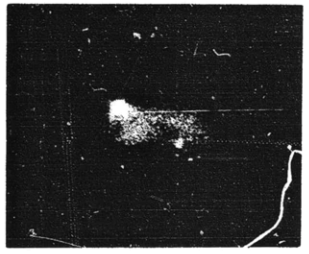

1839:40

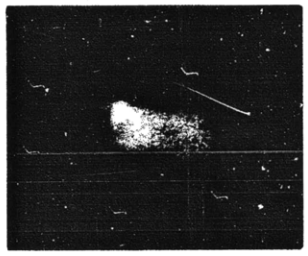

1839:52

1840:05

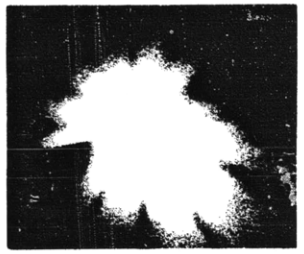

1842:17

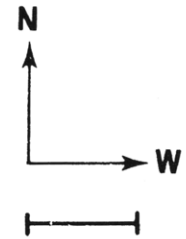

1 arc min.

AR 708 JANUARY 19, 1974 S-054